Supplementary Materials for

Why is Mechanical Fatigue different from Toughness in Elastomers? The Role of Damage by Polymer Chain Scission

Gabriel E. Sanoja*, Xavier P. Morelle, Jean Comtet, C. Joshua Yeh, Matteo Ciccoti, and Costantino Creton

Corresponding author. Email: gabriel.sanoja@espci.psl.eu

This PDF file includes:

Materials and Methods

Materials

Ethyl acrylate (EA), 1,4-butanediol diacrylate (BDA) and 2-hydroxy-2-methylpropiophenone (HMP) were purchased from Sigma-Aldrich. EA and BDA were eluted over activated alumina, whereas HMP was used as received. The mechanofluorescent π-extended anthracene maleimide probe (DACL) was synthesized and purified according to previously established procedures (*1*). All reagents were sparged with N_2 for 45 min and transferred to a N_2-filled glovebox.

Synthesis of SN Elastomers

Filler networks were synthesized via UV-initiated bulk polymerization of EA. In a N_2-filled glovebox; monomer EA, co-crosslinkers BDA and DACL, and initiator HMP were well-mixed in a scintillation vial and subsequently transferred to a mold composed of two PET-covered glass plates sealed with a silicone spacer ($\approx$ 0.1 mm). Polymerization was conducted for 2 h under UV-irradiation (10 μm.cm^{-2}), and the resulting single networks dried overnight at 50 ^{o}C under vacuum. Detailed compositions of the filler networks are summarized in Table S1.

Synthesis of DN Elastomers

In a N_2-filled glovebox; filler networks were swollen to equilibrium in a solution of monomer EA (99.98 mol%), crosslinker BDA (0.01 mol%), and initiator HMP (0.01 mol%) and subsequently transferred to a mold composed of two PET-covered glass plates. Polymerization was conducted for 2 h under UV-irradiation (10 μm.cm^{-2}), and the resulting double networks dried overnight at 50 ^{o}C under vacuum.

Uniaxial Deformation

DN elastomers were punchcut into dogbone-shape specimens of 20 mm length, 4 mm width, and $\approx$ 1.4 mm thickness as defined by the swelling ratio of the filler network. These were marked with two dots of white paint and subsequently deformed at 1.0 mm.s^{-1} (0.05 s^{-1}) with an Instron 5965 equipped with a 100 N load cell and a video extensometer.

Fracture under Monotonic Loading

DN elastomers were cut into pure shear specimens of $\approx$ 30 mm length, and $\approx$ 1.4 mm thickness as defined by the swelling ratio of the filler network. These were marked with two dots of white paint and subsequently loaded on an Instron 5965 equipped with a 100 N load cell and with crossheads separated by 14.5 mm. Specimens were deformed at a crosshead speed of 0.73 mm.s^{-1} (0.05 s^{-1}) while monitoring the stretch with a video extensometer. These experiments were conducted on pristine and pre-cracked specimens (6 mm crack from a fresh razor blade) to determine the applied energy release rate $\mathcal{G}$ as a function of the applied strain λ according to previously established procedures (*2*).

Fracture under Cyclic Loading

DN elastomers were cut into pure shear specimens of $\approx$ 30 mm length, and $\approx$ 1.4 mm thickness as defined by the swelling ratio of the filler network. These were notched with a fresh razor blade and subsequently loaded on a servohydraulic Zwick/Roell Hamsler HC25 equipped with a 5 kN load cell and crossheads covered with millimeter paper. Specimens were deformed

at a displacement-controlled frequency of 10 Hz while monitoring the crack length with a Baumer camera.

Visualization of Damage by Sacrificial Bond Scission

Fractured specimens were cleaned with ethanol and optical paper, taped to a Petri dish, and immersed in glycerol to mitigate refraction at the crack surface. Fluorescent images were acquired on a customized Nikon AZ-100/C2+ confocal macroscope equipped with an AZ Plan Fluor 5x objective of 15 mm focal length. π-Extended anthracene fluorophores were excited with a 405 nm laser and their fluorescent emission recorded in the 424-524 nm range. The optical magnification was set to 5x resulting in 512 x 512 raw images (1.63 μm.px^{-1}) that were subsequently stitched with a 20% overlap. 3-D scans were collected from the specimen surface (*i.e.*, plane of maximum intensity) through a 100 μm depth using a step-size of 10 μm.

Scanning Electron Microscopy

Fractured specimens were imaged with a ThermoFisher Scientific SEM Quattro FEI operating under vacuum at a fixed potential of 5.00 kV.

Supplementary Text

Volume Fraction and Pre-stretch of the Filler Networks

DN elastomers are described by the volume fraction ϕ^{FN} and isotropic pre-stretch λ_0 of the filler network. These were estimated from the mass of single- and double-network elastomers using the following relation:

$$\phi^{FN} = \left(\frac{m_{SN}}{m_{DN}}\right) = \lambda_0^{-1/3} \quad \text{(Eq. S1)}$$

Where m_{SN} and m_{DN} are respectively the mass of single- and double-network.

Maximum Extensibility of the Filler Networks

The maximum extensibility of the polymer chains in the filler network was determined from the chemical crosslink contribution to the shear elastic modulus μ_x of single-network (SN) elastomers $EA_{0.2}$ and $EA_{0.5}$. This was estimated by evaluating the engineering stress within the slip-tube model of Rubinstein and Panyukov (*3*) (Fig. S1):

$$\sigma_N = \mu_x\left(\lambda - \frac{1}{\lambda^2}\right) + \frac{\mu_e\left(\lambda - \frac{1}{\lambda^2}\right)}{0.74\lambda + 0.61\lambda^{-0.5} - 0.35} \quad \text{(Eq. S2)}$$

Where μ_x and μ_e are respectively the contributions of chemical crosslinks and entanglements to the shear elastic modulus. Further consideration of μ_x within rubber elasticity theory enables estimation of the density of elastic strands ν_x and the number of monomers per elastic strand N_x:

$$\mu_x = \nu_x RT = \frac{\rho RT}{M_0 N_x} \quad \text{(Eq. S3)}$$

Where ρ is the polymer density (1.1 g.cm^{-3}), R the ideal gas constant (8.314 J.K^{-1}.mol^{-1}), T the temperature (21 ^{o}C), and M_0 the molecular weight of an ethyl acrylate repeat unit (100.12

g.mol^{-1}). The maximum extensibility of the polymer chain λ_m^{Nx} is then given by the ratio of the contour length and the Gaussian end-to-end distance:

$$\lambda_m^{Nx} = \frac{N_x b}{\sqrt{C_\infty N_x b}} = \sqrt{\frac{N_x}{C_\infty}} \quad \text{(Eq. S4)}$$

Where C_∞ and b are respectively the poly(ethyl acrylate) characteristic ratio (9.3) and bond length (0.204 nm). Results of this analysis are summarized in Table S2 and confirm that the polymer chains of $EA_{0.2}$ are indeed more extensible than those of $EA_{0.5}$. This molecular picture captures the well-known trade-off between stiffness and extensibility in unfilled polymer networks even though it assumes that the modulus is governed by the elastic response of an ensemble of monodisperse polymer chains.

Given that the UV-initiated bulk polymerization of EA involves irreversible chemical reactions, the network structure is expected to be rather heterogeneous. As such, we also determined the maximum extensibility of the polymer chains using an empirical model that combines Mooney-Rivlin and Gent parameters to capture softening and hardening (*4*) (Fig. S2):

$$\sigma_N = 2\left(C_1 + \frac{C_2}{\lambda}\right)\frac{1}{1-\frac{J_1}{Jm}}\left(\lambda - \frac{1}{\lambda^2}\right) \quad \text{(Eq. S5)}$$

Where $J_1 = \lambda^2 + \left(\frac{2}{\lambda}\right) - 3$

The reduced Mooney stress $f^*(\lambda)$ is then given by:

$$f^* = \frac{\sigma_N}{\left(\lambda - \frac{1}{\lambda^2}\right)} = 2\left(C_1 + \frac{C_2}{\lambda}\right)\frac{1}{1-\frac{J_1}{Jm}} \quad \text{(Eq. S6)}$$

This is a convenient way to characterize deviations from rubber elasticity theory given that f^* is constant within this framework. Any dependence of f^* on λ can be interpreted as a signature of entanglements, finite extensibility, or viscoelastic relaxation. This representation can, in principle be used for any material with mechanical behavior governed by entropic elasticity, such as DN elastomers. Results of this analysis are summarized in Table S3 and confirm that the polymer chains of $EA_{0.2}$ are more extensible than those of $EA_{0.5}$. Noteworthy, both filler networks exhibit a maximum extensibility larger than that determined with the slip-tube model of Rubinstein and Panyukov. This observation indicates that the filler networks indeed have heterogeneous structures with densely crosslinked regions interconnected by loosely crosslinked polymer chains.

Areal Chain Density of the Filler Networks and Energy Dissipated by Covalent Bond Scission

Consider an arbitrary plane in a unit volume of polymer network with crosslink density ν_x and Gaussian chains with end-to-end distance $<R_0^2>^{1/2}$. The areal density of polymer chains Σ_0^{FN} crossing the plane is then given by:

$$\Sigma_0^{FN} = \frac{1}{2}\nu_x < R_0^2 >^{1/2} = \frac{\nu_x\sqrt{C_\infty N_x b}}{2} \quad \text{(Eq. S6)}$$

Due to the isotropic swelling of the filler network upon dilution with the matrix, the areal density of filler network chains in the DN elastomer is then given by:

$$\Sigma_0 = \phi^{FN\,2/3}\Sigma_0^{FN} \qquad \text{(Eq. S7)}$$

Results are summarized in Table S4 and can be used to estimate the amount of energy dissipated by covalent bond scission according to the Lake-Thomas theory of fracture:

$$\Gamma_0 = N_x U_b \Sigma_0 \qquad \text{(Eq. S8)}$$

Where U_b is the energy stored per C-C bond along the stretched polymer backbone (60 kJ.mol^{-1}). This prediction is significantly below the fracture energy G_c due to dissipation by viscoelastic processes as well as breakage of more than one monolayer of polymer chains upon crack growth.

Pure Shear Fracture Tests and Energy Release Rate

Pure shear fracture tests were pioneered by Rivlin and Thomas to investigate the fracture of filled rubbers. As discussed in their seminal contribution (*2*), the energy release rate is independent of crack length and given by:

$$G = \bar{W}(\lambda_S)H_0 \qquad \text{(Eq. S9)}$$

Where $\bar{W}(\lambda_S)$ is the strain energy density in the bulk, λ_S the applied deformation, and H_0 the specimen height. We determined $\bar{W}(\lambda_S)$ by evaluating the area under the stress-strain curve of a pristine specimen up to the deformation applied to a pre-cracked specimen fractured under monotonic or cyclic loading (Fig. S4). Detailed deformations, energy release rates, and crack growth rates are summarized in Table S5. Noteworthy, $EA_{0.2}EA$ requires larger deformations than $EA_{0.5}EA$ to attain the same energy release rate because of the softer nature of its filler network. This is important given that the scission of sacrificial bonds is anticipated to be strain dependent.

Quantification of Damage by Sacrificial Bond Scission

Calibration

The fluorescent intensity was calibrated with poly(ethyl acrylate) (PEA) melts of well-known concentration of π-extended anthracene. These were prepared by dissolving (9-phenylethynylanthracene) in a solution of PEA (M_w ~ 95,000 g.mol^{-1}, 18-22 wt% in toluene), drop-casting in a Petri-dish, and allowing the solvent to evaporate for 24 h at room temperature and overnight under vacuum at 50 ^{o}C. The fluorescence originating from (9-phenylethynylanthracene) in PEA was assumed to be analogous to that of damage-activated π-extended anthracene in DN elastomers because of the chemical similarities of the fluorophores and matrices. Measurement of the fluorescence intensity over a range of concentrations enables construction of the following linear calibration curve (Fig. S7):

$$I = I_0 + \alpha c \qquad \text{(Eq. S10)}$$

Where I_0 and is the background fluorescence of PEA, α a linear coefficient, and c the concentration of (9-phenylethynylanthracene).

Illumination inhomogeneities and electronic noise

Illumination inhomogeneities due to low magnification of the confocal macroscope were evident at the edges of raw images, and overlapped areas of stitched images. This *vignetting* artifact was mitigated by restricting the analysis to a centered region-of-interest while stitching with a 20% overlap (Fig. S8).

Electronic noise was subsequently removed by subtracting a dark image acquired at the same laser power and gain and then applying a median filter.

Quantification

The per-voxel fraction of π-extended anthracene moieties ϕ_{xyz} was determined from the fluorescence intensity I_{xyz}:

$$\varphi_{xyz} = \frac{c_{xyz} V N_A}{c_0} = \frac{I_{xyz}}{\alpha c_0} V N_A \qquad \text{(Eq. S11)}$$

Where c_0 is the per-voxel concentration of π-extended anthracene-maleimide adducts prior fracture, V the volume of a voxel (32.06 μm^3), and N_A Avogadro's number. The analysis was restricted to a distance from the crack edge L of 300 μm to mitigate vignetting artifacts, and any activation beyond 255 μm was attributed to the background (Fig. S8-S9). This is equivalent to neglecting any bulk damage, an assumption justified by the absence of mechanical hysteresis in a step-cyclic load until failure (Fig. S3). The fraction of bonds broken in the filler network at a distance y from the crack surface ϕ_y, the local damage per unit area of crack propagation $\overline{\Sigma_{xz}}$, and the overall damage per unit area of crack propagation $\bar{\Sigma}$ can then be calculated with Eq. 1-3.

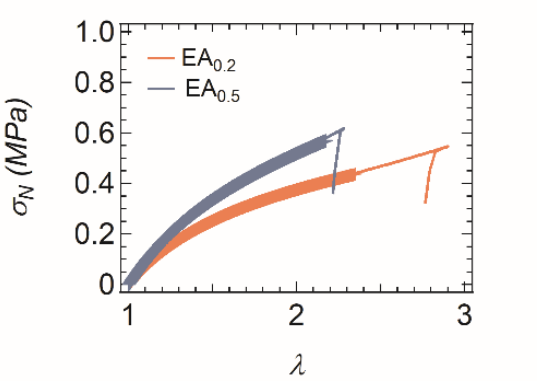

Fig. S1.

Uniaxial deformation of SN elastomers. EA$_{0.2}$ and EA$_{0.5}$ exhibit a stress softening characteristic of entangled polymer networks and well-described by a slip-tube model (+)

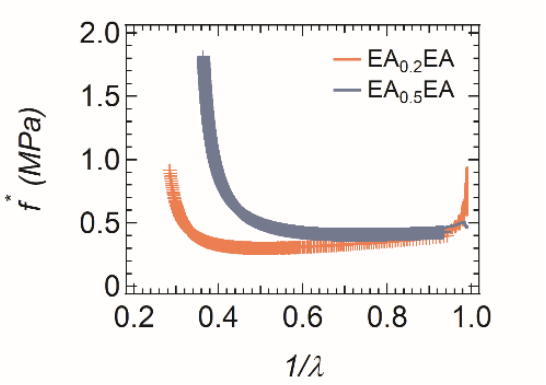

Fig. S2.

Mooney plot of DN elastomers. $EA_{0.2}EA$ and $EA_{0.5}EA$ exhibit an increase in reduced stress at large strains, a behavior characteristic of elastomers with polymer chains near their maximum extensibility.

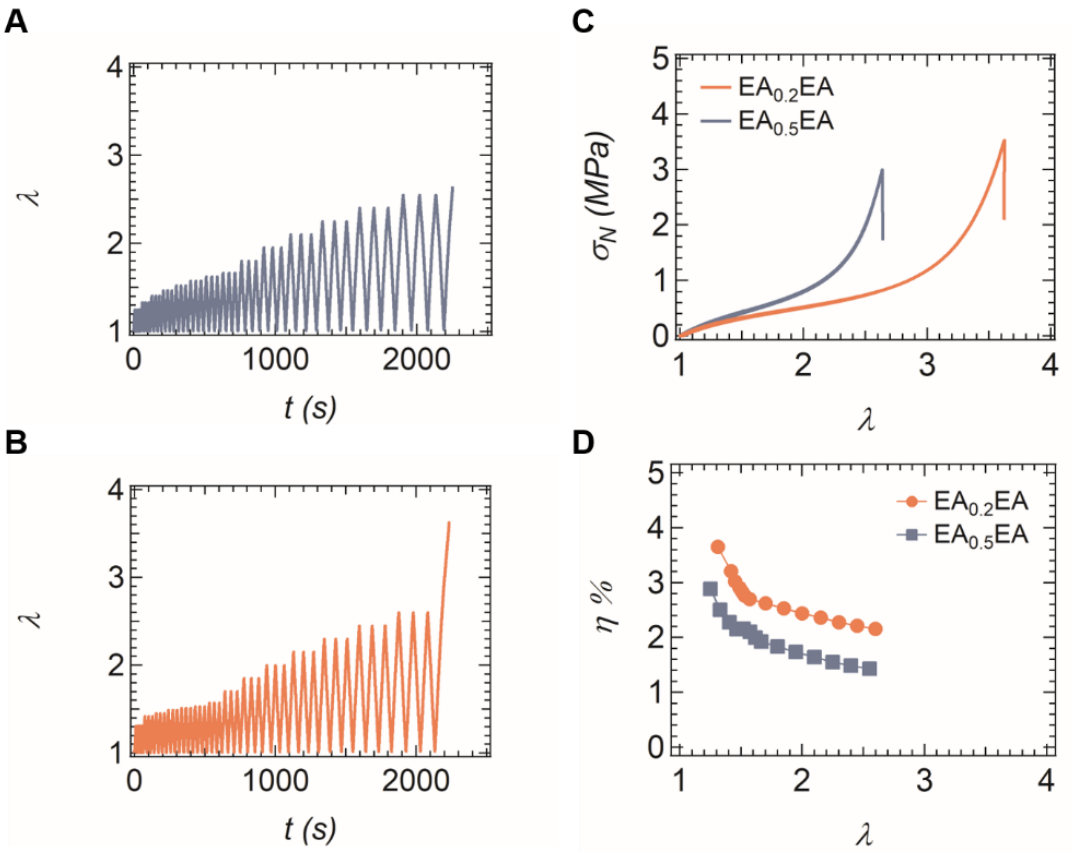

Fig. S3.

Cyclic deformation of DN elastomers. Strain wave of (**A**) $EA_{0.5}EA$ and (**B**) $EA_{0.2}EA$. (**C**) Stress-strain curves reveal negligible mechanical hysteresis in DN elastomers. This observation is consistent with the low (**D**) fraction of energy dissipated relative to the work of deformation.

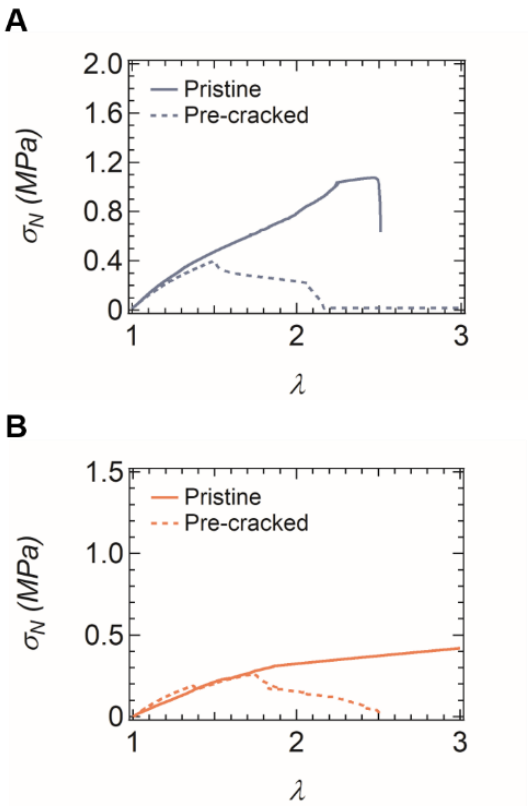

Fig. S4.

Pure shear fracture tests of DN elastomers. (**A**) $EA_{0.5}EA$ and (**B**) $EA_{0.2}EA$ exhibit overlapping stress-strain curves in pristine and pre-cracked specimens up to the critical stretch. The applied energy release rate is determined with the strain energy density in the pristine specimen at the deformation imposed to the pre-cracked specimen.

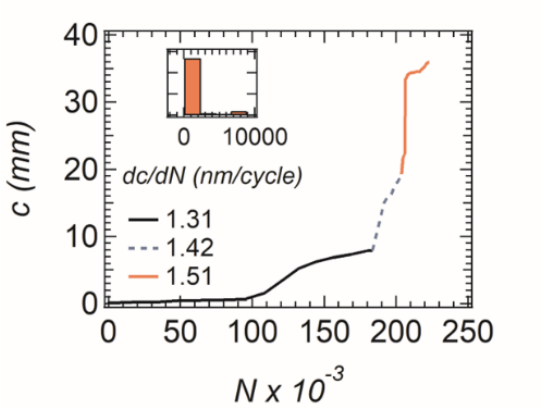

Fig. S5.

Fatigue crack propagation of DN elastomers. (**A**) Crack growth of $EA_{0.2}EA$ is discontinuous and dependent on the applied stretch λ and energy release rate $\mathcal{G}(\lambda)$. (Inset) Representative distribution of crack growth rates *dc/dN* for $\lambda = 1.51$ or $\mathcal{G}(\lambda) = 727$ J.m^{-2}.

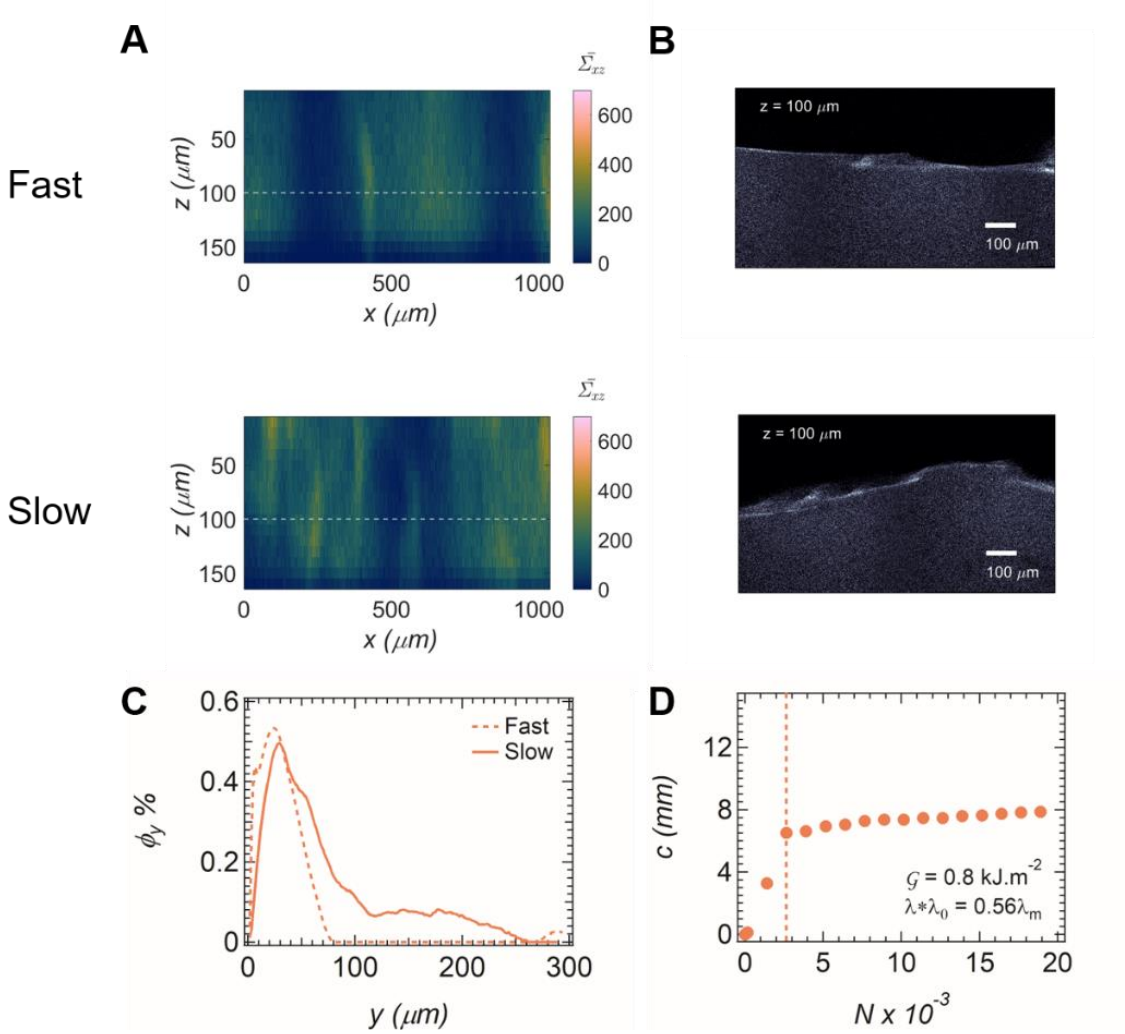

Fig. S6.
Damage of $EA_{0.2}EA$ fractured under cyclic loading at $\mathcal{G} \approx 0.8$ kJ.m^{-2}. (**A**) Spatial maps of local damage per unit area of crack propagation $\overline{\Sigma_{xz}}$ reveal that $EA_{0.2}EA$ is slightly more damaged in the *slow* than in the *fast* crack growth regime. (**B**) Representative images at z = 100 μm (white dashed line in Fig. S6A) illustrate that crack bifurcations are associated with hotspots in damage maps. (**C**) Profiles of ϕ_y reveal that $EA_{0.2}EA$ undergoes catastrophic failure due to sudden localization of damage ahead of the crack tip. (**D**) Crack growth of $EA_{0.2}EA$ at $\mathcal{G} \approx 0.8$ kJ.m^{-2}. The crack growth transitions from the *fast* to the *slow* regime at the critical number of cycles N_c (dashed vertical line).

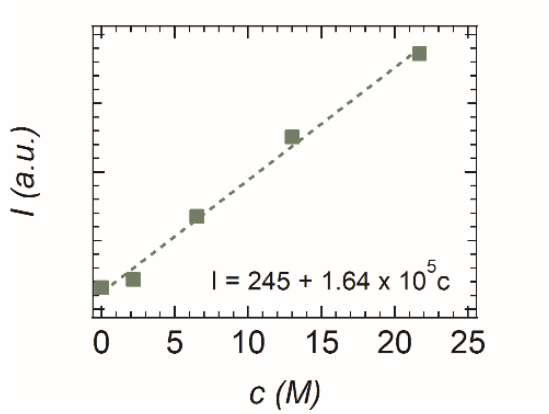

Fig. S7.

Calibration of fluorescence intensity with concentration of (9-phenylethynylanthracene) probe in a PEA matrix. Linear relation between intensity and concentration enables quantification of damage by sacrificial bond scission in DN elastomers.

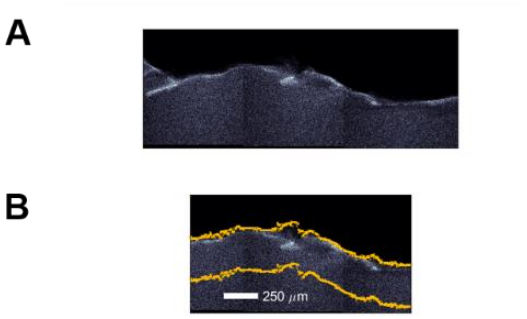

Fig. S8.

Image processing for quantification of damage by sacrificial. (**A**) Raw image exhibits illumination inhomogeneities at the edges and stitching areas. These artifacts were mitigated by restricting the analysis to a (**B**) centered region-of-interest.

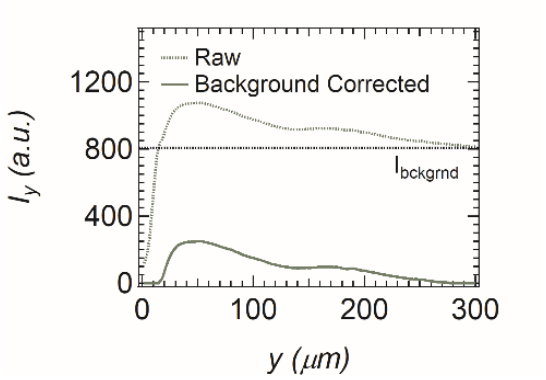

Fig. S9.

Background correction of the fluorescent intensity. The background intensity was defined as the mean from 250 μm to 300 μm. This is equivalent to neglecting any bulk activation of the mechanofluorescent probe, an assumption justified by the negligible hysteresis of DN elastomers under step-cyclic loading (Fig. S3).

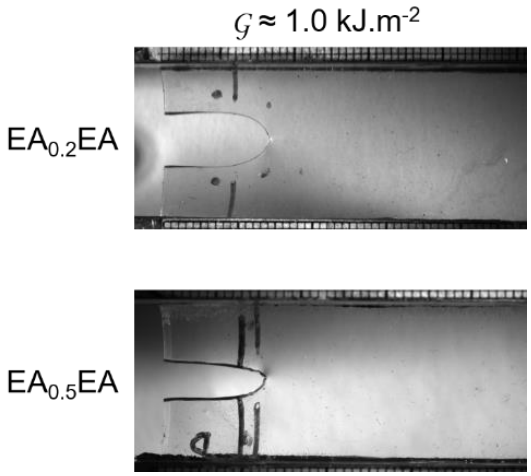

Fig. S10.

Images of DN elastomers fractured under cyclic loading at $\mathcal{G} \approx 1.0$ kJ.m^{-2}. In the open configuration, the crack is more blunted in $EA_{0.2}EA$ than in $EA_{0.5}EA$ at somewhat similar bulk strains λ.

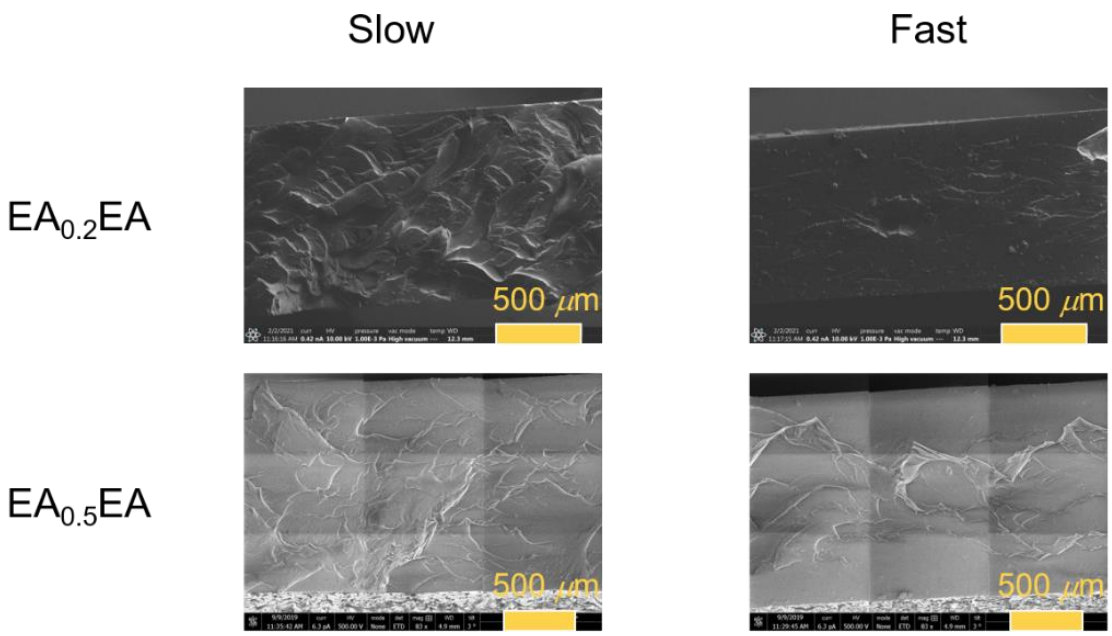

Fig. S11.

SEM of DN elastomers fractured under cyclic loading. The fracture surface is rougher in the *slow* than in the *fast* crack growth regime.

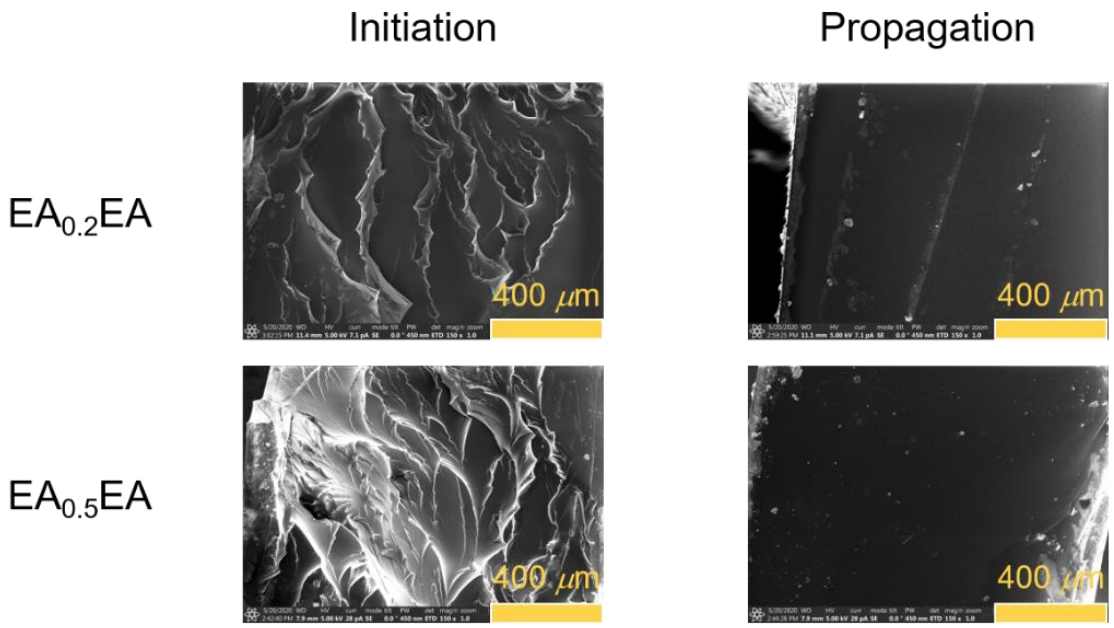

Fig. S12.

SEM of DN elastomers fractured under monotonic loading. Fracture surface is rougher in the *initiation* than in the *propagation* regime.

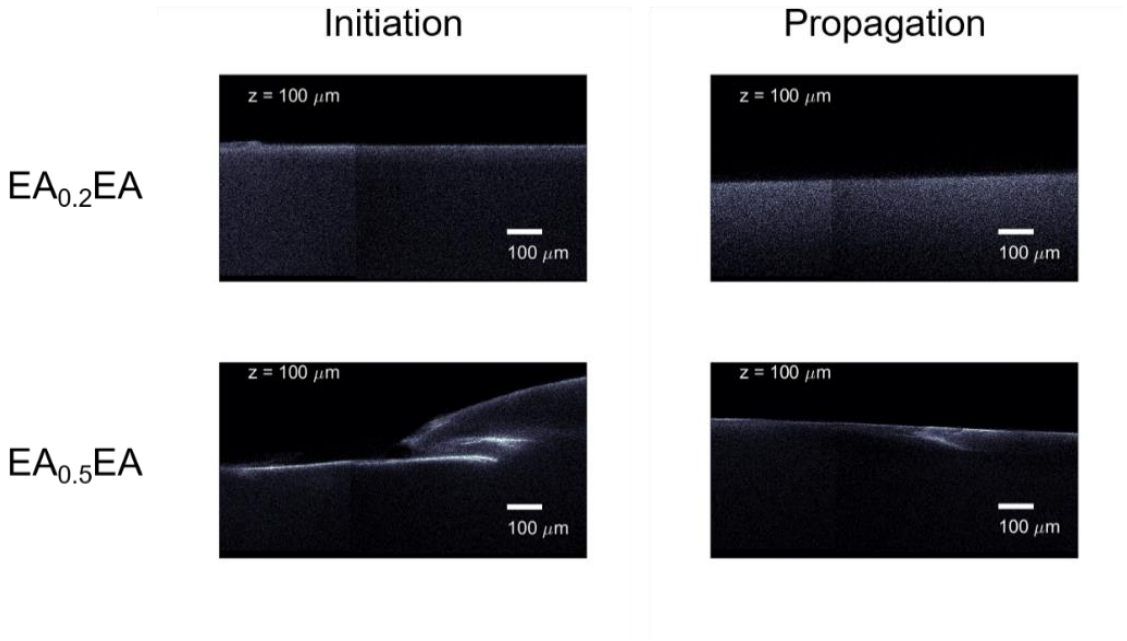

Fig. S13.

Fluorescent images of DN elastomers fractured under monotonic loading (white dashed lines in Fig. 8A). Crack bifurcations are evident in the *initiation* and *propagation* regime of EA-$_{0.5}$EA and associated with hotspots in Fig. 8A.

Table S1.
Composition of the filler networks.

	EA (mol%)	BDA (mol%)	DACL (mol%)	HMP (mol%)	Load
$EA_{0.2}$	98.640	0.175	0.025	1.160	Monotonic
$EA_{0.2}$	98.640	0.190	0.010	1.160	Cyclic
$EA_{0.5}$	98.340	0.475	0.025	1.160	Monotonic
$EA_{0.5}$	98.340	0.475	0.025	1.160	Cyclic

Table S2.

Estimation of the maximum extensibility of the filler networks with the slip-tube model. Consideration of the nominal stress within the slip-tube Rubinstein-Panyukov model provides the respective contributions of chemical crosslinks and entanglements to the shear elastic modulus. These can be used to estimate the maximum extensibility of polymer chains using the affine approximation of rubber elasticity theory.

	μ_x *(MPa)*	μ_e *(MPa)*	ν_x *(chains.m^{-3})*	N_x	λ_m^{Nx}
EA$_{0.2}$	0.11	0.17	2.6 x 10^{25}	253	5.22
EA$_{0.5}$	0.20	0.15	4.9 x 10^{25}	135	3.80

Table S3.

Estimation of the maximum extensibility of the filler networks with an empirical model that combines a Mooney-Rivlin softening with a Gent hardening.

	C_1 (MPa)	C_2 (MPa)	J_m	λ_m	$\lambda_m^{MR\text{-}G}$
$EA_{0.2}EA$	0.05	0.16	12.37	3.85	6.70
$EA_{0.5}EA$	0.12	0.10	6.39	2.95	4.89

Table S4

Estimation of the areal chain density and Lake-and-Thomas fracture energy of polymer chains in the filler network.

	Σ_0^{FN} (chains.m^{-2})	Σ_0 (chains.m^{-2})	Γ_0 (J.m^{-2})
EA$_{0.2}$EA	1.8 x 10^{17}	6.0 x 10^{16}	1.5
EA$_{0.5}$EA	2.5 x 10^{17}	9.2 x 10^{16}	1.2

Table S5

Loading conditions and crack growth rates of fatigue fractured DN elastomers. Presented are the applied stretch λ, applied stretch to the filler network $\lambda*\lambda_0$, energy release rate $\mathcal{G}$, and crack growth rate *dc/dN*.

	λ	$\lambda*\lambda_0$	$\mathcal{G}$ ($J.m^{-2}$)	$dc/dN \times 10^5$ ($mm.cycle^{-1}$)
$EA_{0.2}EA$	1.31	2.28	290.2	4.92
	1.42	2.47	531.6	59.6
	1.51	2.63	726.8	384
	1.51	2.63	726.8	14.2
	1.45	2.53	606.5	11.4
	1.49	2.59	807.6	144
	1.49	2.59	807.6	6.40
	1.53	2.66	871.9	24.6
	1.57	2.72	956.1	6800
$EA_{0.5}EA$	1.25	2.09	545.2	0.21
	1.33	2.22	931.8	1.27
	1.41	2.35	1304	3.78
	1.47	2.45	1642	6.91
	1.52	2.54	1819	13.6
	1.52	2.54	1328	3.33
	1.58	2.63	1843	5.91
	1.62	2.71	2069	161
	1.62	2.71	2069	20.0
	1.67	2.78	2392	0.54
	1.67	2.78	2392	5260

Movie S1.

Fatigue crack propagation of $EA_{0.5}EA$ at $\mathcal{G} = 2069\ J.m^{-2}$. *Fast* and *slow* crack growth regimes coexist with distinct *dc/dN*.

Movie S2.

Fatigue crack propagation of $EA_{0.2}EA$ at $\mathcal{G} = 808\ J.m^{-2}$. *Fast* and *slow* crack growth regimes coexist with distinct *dc/dN*.

Movie S3.

Fracture under monotonic loading of $EA_{0.5}EA$. An *initiation* regime of slow crack growth precedes *propagation*..

Movie S4.

Fracture under monotonic loading of $EA_{0.2}EA$. An *initiation* regime of slow crack growth precedes *propagation*..

References

1. R. Göstl, R. P. Sijbesma, π-extended anthracenes as sensitive probes for mechanical stress. *Chem. Sci.* **7**, 370–375 (2016).
2. R. S. Rivlin, A. G. Thomas, in *Collected Papers of R.S. Rivlin* (Springer New York, New York, NY, 1997; http://link.springer.com/10.1007/978-1-4612-2416-7_180), vol. X, pp. 2615–2642.
3. M. Rubinstein, S. Panyukov, Elasticity of polymer networks. *Macromolecules*. **35**, 6670–6686 (2002).
4. L. Léger, C. Creton, Adhesion mechanisms at soft polymer interfaces. *Philos. Trans. R. Soc. A Math. Phys. Eng. Sci.* **366**, 1425–1442 (2008).